Simulation of Primary Breakup for Diesel Spray with Phase Transition

Peng Zeng[1], Samuel Sarholz[2], Christian Iwainsky[2], Bernd Binninger[3], Norbert Peters[3], and Marcus Herrmann[4]

[1] Institut for Combustion Technology
RWTH Aachen University
Templergraben 64, 52056 Aachen, Germany
Tel.: +49-241 80-94622
Fax: +49-241 80-92923
p.zeng@itv.rwth-aachen.de
[2] Center for Computing and Communication
RWTH Aachen University
sarholz@rz.rwth-aachen.de
[3] Institut for Combustion Technology
RWTH Aachen University
[4] Department of Mechanical and Aerospace Engineering
Arizona State University
marcus.herrmann@asu.edu

Abstract. We perform direct numerical simulation on large distributed memory parallel computers in order to investigate the primary breakup process of diesel spray direct injection. Local refinement algorithm–Refined level–set method has been used to reduce the memory requirement, and we analyze the performance by experiments on a 1024–processor parallel computer.

Keywords: Two–phase flow, Liquid atomization, DNS.

1 Introduction

Numerical simulation of diesel engine combustion has become an important tool in engine development. One major issue in the modeling of turbulent reactive flows is the turbulent spray that accompanies fuel injection. The atomization of a liquid jet can be considered as two subsequent processes: Primary breakup, also called primary atomization, is the very first fragmentation process when the liquid column rushes out of a nozzle, forming ligaments and breaking up into primary droplets. Then, the spray will continue to break up into smaller droplets, this is called the secondary atomization process. The small droplets will evaporate, forming fuel–air mixture, ultimately, ignition will start combustion. Among all the physical models of the spray combustion process, the primary breakup of liquid jets in an initial dense region is mostly poorly understood due to its complex nature [7], as it involves a sudden jump in the density across the

M. Ropo et al. (Eds.): EuroPVM/MPI 2009, LNCS 5759, pp. 313–320, 2009.

gas-liquid interface, surface tension force on the interface, topological changes of the interface, and phase transition.

Modeling primary atomization has so far relied on analytical and empirical approaches. They predict mean drop sizes and global primary breakup rates, but mostly fail to capture the interaction of the phase interface with the turbulent flow field on the numerically resolved scale.

Different from traditional approaches, we consider using direct numerical simulation(DNS) combined with level–set method to resolve all time and length scales of primary atomization close to the injector [1]. By solving the governing equations in all details and capturing the gas-liquid interface accurately, we may provide new understanding towards the physics of primary atomization. The detailed information shall be used to derive a statistical model to simulate primary breakup for engineering application.

In the following sections, firstly, in section 2, the governing equations and the refined level-set grid method will be described. Then, the computational aspects concerning the performance of the numerical method will be discussed in section 4. In section 3, we will cover the direct numerical simulation of primary breakup with some interesting result.

2 Two-Phase Flow Using Level-Set Method

The two-phase flow is described in one-fluid formulation, liquid and vapor phases have their own fluid properties, i.e., density, viscosity, surface tension, etc. The flow is governed by the unsteady Navier-Stokes equations in the variable density incompressible limit[1,7],

$$\nabla \cdot \boldsymbol{u} = 0 \tag{1}$$

$$\frac{\partial \boldsymbol{u}}{\partial t} + \boldsymbol{u} \cdot \nabla \boldsymbol{u} = -\frac{1}{\rho}\nabla p + \frac{1}{\rho}\nabla \cdot (\mu(\nabla \boldsymbol{u} + \nabla^T \boldsymbol{u})) + \boldsymbol{g} + \frac{1}{\rho}\boldsymbol{T}_\sigma \tag{2}$$

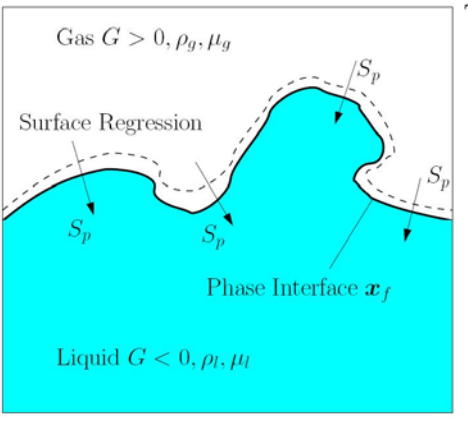

Fig. 1. G field

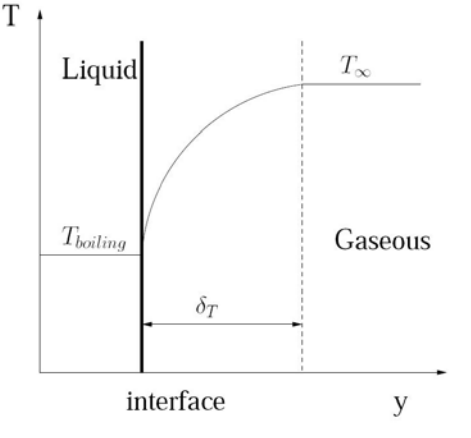

Fig. 2. Temperature Boundary Layer

Surface tension force $\boldsymbol{T}_\sigma$ is non-zero only at the location of the phase interface $\boldsymbol{x}_f$

$$\boldsymbol{T}_\sigma(\boldsymbol{x}) = \sigma\kappa\delta(\boldsymbol{x} - \boldsymbol{x}_f)\boldsymbol{n} \quad . \tag{3}$$

The phase interface location $\boldsymbol{x}_f$ is described by a level–set scalar $G(\boldsymbol{x}_f, t) = 0$.In the gas, $G(\boldsymbol{x}_f, t) < 0$; in the liquid, $G(\boldsymbol{x}_f, t) > 0$. The surface regression velocity S_p shown in Fig. 1 due to evaporation, leads to the interface evolution equation as

$$\frac{\partial G}{\partial t} + \boldsymbol{u} \cdot \nabla G + S_P|\nabla G| = 0 \quad . \tag{4}$$

Starting from the balance of energy, we assume all the conducted heat is consumed by evaporation,

$$\frac{\rho_g \nu_g}{Pr}\frac{\partial T}{\partial y} = \frac{\dot{m} h_L}{C_p} \quad , \tag{5}$$

where $\dot{m} = \rho_l S_p$ is the mass flow rate per unit area, h_L is the latent heat of phase transition, C_p is the heat capacity of liquid phase, and Pr is the Prandtl number. Fig. 2 shows the temperature boundary layer, where δ_T is the boundary layer thickness which includes the length scale. In laminar cases, the surface regression velocity can therefore be modeled as

$$S_p = \frac{1}{P_r}\frac{\rho_g}{\rho_l}\frac{C_p(T_\infty - T_{Boiling})}{h_L}\frac{\nu_g}{\delta_T} \quad . \tag{6}$$

3 Numerical Methods

The primary breakup process contains a large range of physical length scales, ranging from the size of the jet or sheet down to the size of the tiny drops that can be initially ripped out of the phase interface. Adaptive mesh refinement techniques are essential to ensure correct DNS results, using available computing resources. The interface evolution equation (4) is solved by using Refined Level-Set Grid(RLSG) method on an auxiliary, high-resolution equidistant Cartesian grid(see Fig. 3), while the Navier-Stokes equations (1)(2) are solved on their own

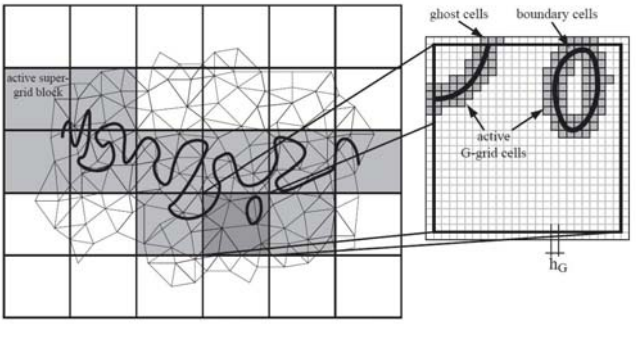

Fig. 3. Refined Level Set Grid method

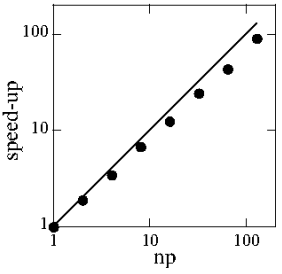

Fig. 4. Speedup of RLSG method [2]

computational grid. The remaining variables are expressed in terms of function based on the instantaneous position of the liquid-vapor interface. The RLSG solver LIT (Level set Interface Tracker) uses 5th order WENO scheme for space and 3rd order Runge-Kutta scheme for time discretization. The Navier-Stokes equations are spatially discretized using low-dissipation, finite-volume operators [3]. The flow solver CDP uses a fully unstructured computational grid. A low-dissipation, finite-volume operators [3] spatially discretized the Navier-Stokes equations. CDP uses a second order Crank-Nicolson scheme for implicit time integration, and the fractional step method will remove the implicit pressure dependence in the momentum equations. Communication between the level–set solver and the flow solver is handled by the coupling software CHIMPS [4]. Domain decomposition parallelization of RLSG method has been achieved by the two–level narrow band methodology. On the first level, the super–grid cells, or blocks, that contain part of the interface are activated and stored in linked lists distributed among the distributed processors (see Fig. 3). A lookup table stores the i, j, k coordinates of the super–grid coordinates enable fast access of them. On the second level, each active block contains an equidistant Cartesian grid of local refined grid size h_G (see Fig. 3). Again, only those grid cells that contain part of the interface are activated and stored. This approach effectively reduces the number of cells that are stored and on which the level–set equations have to be solved from $O(N^3)$ to $O(N^2)$. Moreover, the dynamic load balancing and direct access to random nodes are straightforward, so high level of parallel efficiency and scalability can be achieved (see Fig.4).

4 Computational Aspects

The simulation has been computed on an Intel Xeon-based Linux cluster at the Center for Computing and Communication of the RWTH Aachen University. The 128 nodes are equipped with two 3 Ghz Xeon E5450 quad-core processors and 16 GB of memory and are connected with 4x DDR Infiniband.

The dataset uses approximately 100 GB of memory, which is evenly split between the MPI processes. Overall 6000 time steps were computed with 512 processes on 128 nodes using a wall-clock time of 51 hours. Lacking a serial run for the large data set, we approximate a speedup of 350.

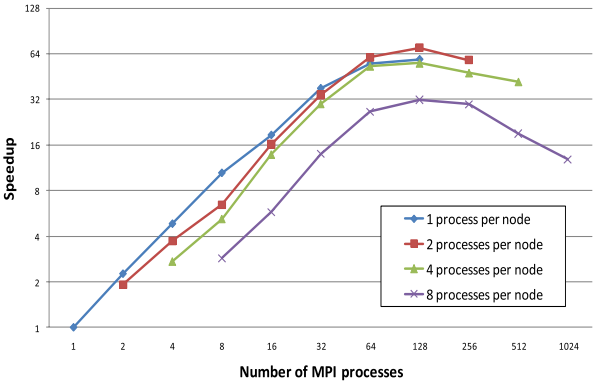

Fig. 5. Scalability graph, reduced data set

We concluded that the original dataset was too large to be usable for speedup measurements due to memory restrictions. Therefore we scaled the data set down by a factor of 8 and computed only two iterations.

With measurement we determined that the optimal performance (70.2 speedup) was reached with 128 MPI processes, see figure 5. For small MPI process numbers, in this case 32, we observed superlinear speedup as a benefit of accumulated cache size. Evaluation of the communication behavior with Vampir [8] showed, that the increasing complexity of the mainly used allreduce dominates the execution time for more than 128 processes.

Variation of the number of processes per node did not change the behavior of the scalability. The optimal number of processes per node is about 2 or 4, as the memory bandwith of a single node reaches saturation for this.

We can only partially measure the scalability of the large data set. Therefore we compared samples of the speedup curve for the large dataset starting at 32 MPI processes through 512 with the smaller one. We observe that the sampled area shows same characteristics as the scaled version shifted by a factor of 8. Extrapolating from the available speedup curves we predict that the large data set will reach its lowest execution time with 1024 MPI processes running on 512 nodes.

5 DNS Results of Primary Breakup

The simulations use $256 \times 256 \times 512$ grid points in radial, azimuthal and axial directions for the flow solver, and the mesh is stretched in order to cluster grid points near the spray center, spacing the finest grid $\Delta x \simeq 3\eta \sim 4\eta$, where $\eta \simeq 1\mu m$ is the Kolmogorov length coherent to the Reynolds number given before. The refined level–set grid has a half billion active cells. This combination was shown to yield promising results for primary breakup [5] [4].

Fig. 6 shows snapshots of the turbulent liquid jet and droplets generated by primary breakup. The Lagrangian spray model, which removes the droplets from

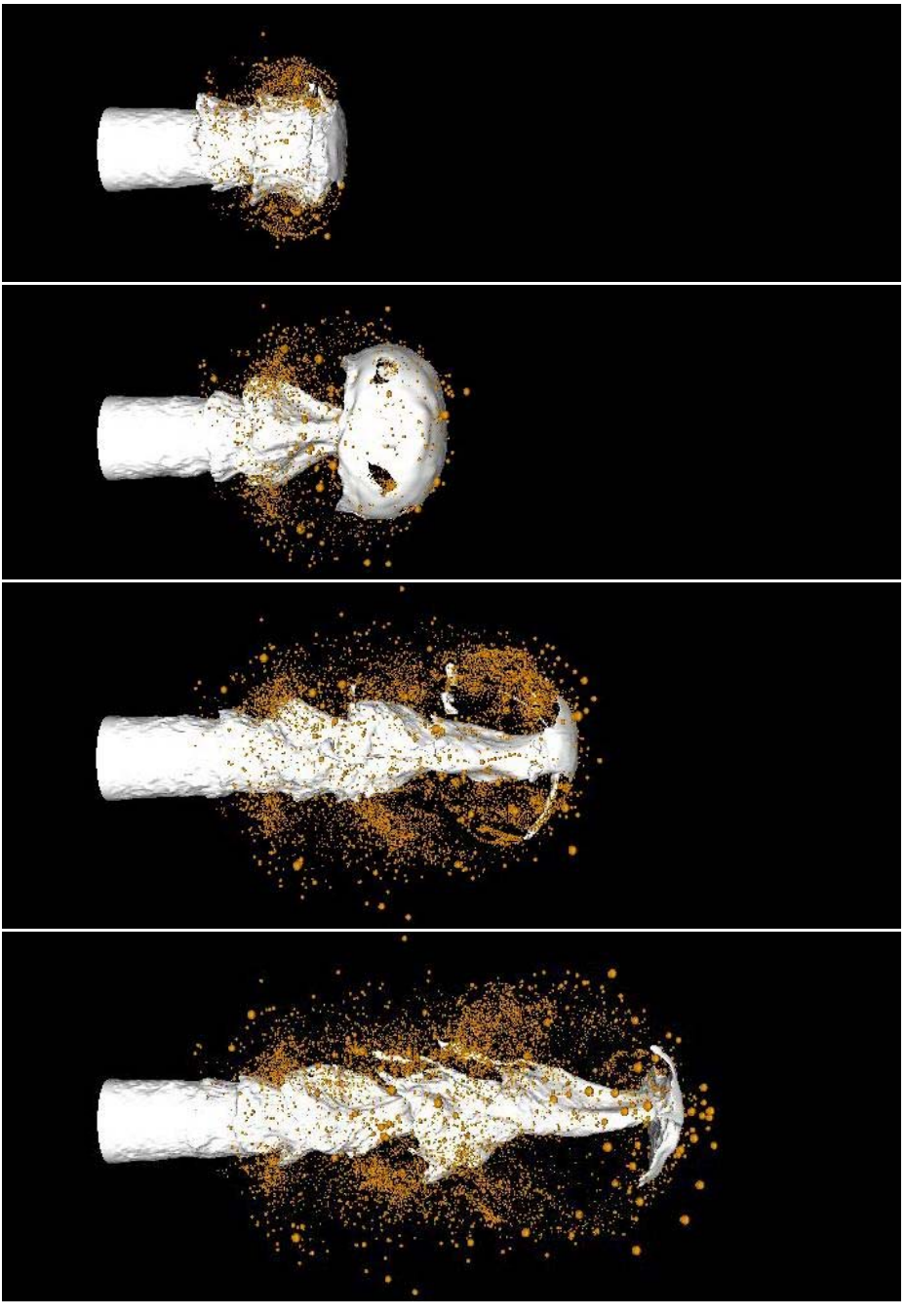

Fig. 6. Four successive snapshots of primary atomization, from top to bottom, $t = 4\mu s$, $t = 6\mu s$, $t = 8\mu s$, $t = 10\mu s$

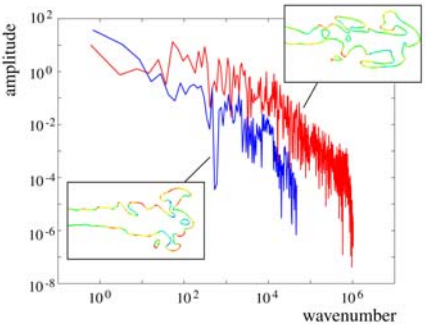

Fig. 7. Curvature Spectrum, with evaporation(red), without(blue)

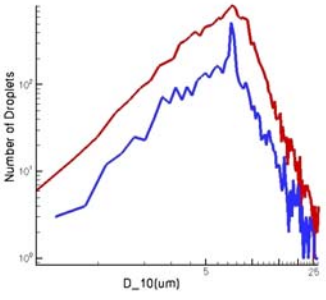

Fig. 8. Droplet size distribution, with evaporation(red), without(blue)

the ligaments and transfers into Lagrangian particles, can be found in [5]. Most of the droplets come from the mushroom tip at the jet head, complex topology and elongated ligaments have been observed. Compared with the atomization process without evaporation, the breakup of ligaments and droplet generation are much faster and more intensive. This can be explained in Fig. 7, which shows the curvature spectrum made from Fourier transformation of local curvature values along the ligaments with- and without evaporation. In the evaporation case, the large wave number of curvature fluctuations will promote the breakup processes.

Fig. 8 shows the droplet size distribution, ranging from the cut-off length scale that accompanies with the numerical grid size to large liquid blocks. Different from the atomization process without evaporation, more small droplets can be observed. Mesh convergence has not been performed yet, this is a first step in a series of calculations, where the focus is on the evaporation effect on spray primary breakup.

6 Summary and Outlook

The refined level–set grid method for primary breakup with phase transition has been presented. The speedup performance analysis shows that for a constant number of processors best effeciencies are reached when the problem size is as large as possible. However, for every problem with a specific size, there is an optimal number of processors to use. The scalability of our code for the current case was found satisfactory, as we can compute in 4 days for a typical run. The two phase flow solver has been applied on direct numerical simulation of a turbulent diesel injection, although there are many numerical uncertainties, preliminary results show promising direction towards further understanding of the physical process of atomization with evaporation effect. The mathematical model and the DNS solution presented here will provide the frame for a statistical simulation of the primary breakup, within the large eddy simulation (LES) will be done in the future. Investigation is necessary to reduce the MPI overhead

and improve performance in order to be able to couple our code with secondary breakup models, and ultimately towards spray combustion simulation.

Acknowledgments

This work is financed by the German Research Foundation in the framework of DFG-CNRS research unit 563: Micro-Macro Modelling and Simulation of Liquid-Vapour Flows, (DFG reference No. Pe241/35-1).

References

1. Gorokhovski, M., Herrmann, M.: Modeling Primary Atomization. Annual Review of Fluid Mechanics 40, 343–366 (2008)
2. Herrmann, M.: A balanced force Refined Level Set Grid method for two- phase flows on unstructured flow solver grids. J. Comput. Phys. 227, 2674–2706 (2008)
3. Ham, F., Mattsson, K., Iaccarino, G.: Accurate and stable finite volume operators for unstructured flow solvers. Center for Turbulence Research Annual Research Briefs (2006)
4. Kim, D., Desjardins, O., Herrmann, M., Moin, P.: The Primary Breakup of a Round Liquid Jet by a Coaxial Flow of Gas. In: Proceedings of the 2oth Annual Conference of ILASS Americas (2007)
5. Herrmann, M.: Detailed Numerical Simulations of the Primary Breakup of Turbulent Liquid Jets. In: Proceedings of the 21st Annual Conference of ILASS Americas (2008)
6. Spiekermann, P., Jerzembeck, S., Felsch, C., Vogel, S., Gauding, M., Peters, N.: Experimental Data and Numerical Simulation of Common-Rail Ethanol Sprays at Diesel Engine-Like Conditions. Atomization and Sprays 19, 357–387 (2009)
7. Baumgarten, C.: Mixture Formation in Internal Combustion Engines. Springer, Heidelberg (2006)
8. Knüpfer, A., Brunst, H., Doleschal, J., Jurenz, M., Lieber, M., Mickler, H., Müller, M.S., Nagel, W.E.: The Vampir Performance Analysis Tool-Set. In: Proceedings of the 2nd HLRS Parallel Tools Workshop (2008)